JCTC Journal of Chemical Theory and Computation

Article

pubs.acs.org/JCTC

Density Functional Theory and Beyond for Band-Gap Screening: Performance for Transition-Metal Oxides and Dichalcogenides

Wenqing Li, Christian F. J. Walther, Agnieszka Kuc,* and Thomas Heine

School of Engineering and Science, Jacobs University Bremen, Campus Ring 1, 28759 Bremen, Germany

Supporting Information

ABSTRACT: The performance of a wide variety of commonly used density functionals, as well as two screened hybrid functionals (HSE06 and TB-mBJ), on predicting electronic structures of a large class of en vogue materials, such as metal oxides, chalcogenides, and nitrides, is discussed in terms of band gaps, band structures, and projected electronic densities of states. Contrary to GGA, hybrid functionals and GGA+*U*, both HSE06 and TB-mBJ are able to predict band gaps with an appreciable accuracy of 25% and thus allow the screening of various classes of transition-metal-based compounds, i.e., mixed or doped materials, at modest computational cost. The calculated electronic structures are largely unaffected by the choice of basis functions and software implementation, however, might be subject to the treatment of the core electrons.

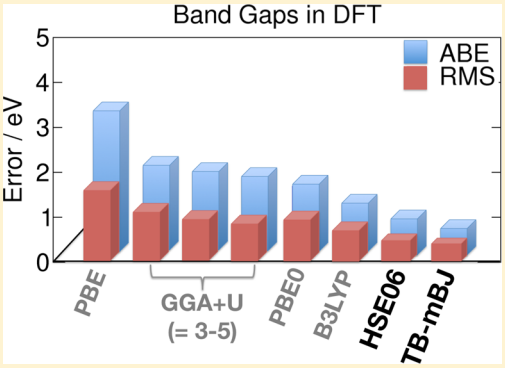

INTRODUCTION

Kohn−Sham density functional theory (DFT)[1,2] has been widely used in the solid-state community for electronic structure calculations. It has been proven to be a competitive method for various ground-state applications in physics, chemistry, and materials science. While DFT is, in principle, an exact approach for ground-state properties, the results strongly rely on the approximation of the exchange correlation (XC) potential that describes the many-body interaction between electrons. The choice of XC is very important, especially for the systems containing transition-metal atoms, such as transition-metal oxides or dichalcogenides, where a systematic evaluation of various density functionals is essential in the fields of, e.g., electronic structure calculations.

Transition-metal dichalcogenides (TMDs) are layered materials with extraordinary electronic properties arising from quantum confinement to lower dimensions. Three-dimensional (3D) TMDs can be either semiconductors or metals, depending on the stoichiometry (e.g., MoS_2 or NbS_2). 3D TMDs are easy to process using liquid exfoliation and large-area single layers can be produced at low costs.[3] While 3D bulk structures are indirect-band-gap semiconductors, the two-dimensional (2D) monolayers are direct-band gap materials.[4] This phenomenon has been utilized to produce the first field-effect transistors, logical circuits, and amplifiers based on the MoS_2 monolayer.[5−7] 2D TMDs are very interesting for future nanoelectrodevices and flexible electronics.

Transition-metal oxide (TMO) semiconductors are technologically very important materials, because they have been recognized for potential applications in energy conversion devices, in particular in photocatalysis, photovoltaics, and photoelectrochemistry.[8−11] TMOs are attractive candidates for large-scale applications as many of them are low-production-cost materials, stable under ultraviolet (UV) light and against chemically aggressive environments, and relatively abundant. Structural, elastic, magnetic, and energetic properties of TMOs have been a subject of numerous investigations and are presently quite well understood.[12−19] However, the correct description of their electronic structure is still incomplete within the existing theoretical models. For a theorist, TMOs are among the most exciting as well as most difficult electronic systems to study, because of the partially occupied d-orbitals of the transition metals, the resulting open-shell nature, appreciable correlation effects, and the variety of spin configurations in a limited energy region.

To evaluate the applicability of TMO-based materials for solar energy conversion devices theoretically, accurate albeit efficient methods are required to determine band-edge positions in the electronic structure as well as the band-gap size. Knowledge of these two properties provides the first crude screening of materials as potentially effective photoelectrodes or photocatalysts. Experimentally obtained band-gap sizes are fairly accurate, while the band-gap edges are usually determined by photoemission spectroscopy, which is subject to defects at the TMO surfaces and, thus, may lead to inaccurate measurements.

Calculations of the electronic band structure of TMOs are challenging, because of the strong interactions between the electrons localized in the d-orbitals. In this case, any electron transfer between the metal ions results in large energy fluctuations and the d-orbitals can be taken into account by neither the localized nor delocalized electron model and, therefore, require special treatment. The most popular

Received: March 25, 2013
Published: May 29, 2013

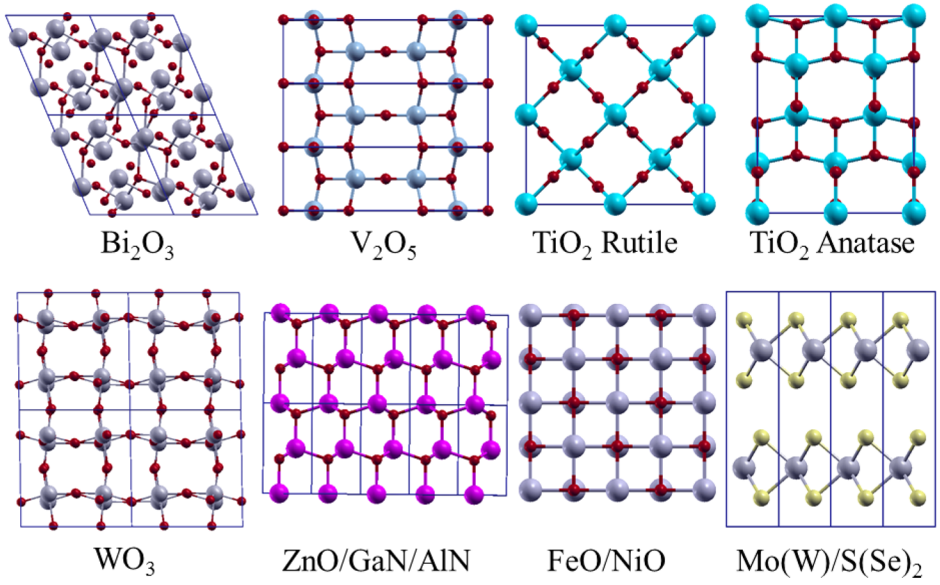

Figure 1. Three-dimensional (3D) supercell representation of the crystal structures studied in the present work.

Table 1. Materials, Their Crystal Class Symmetries, and the Experimental Lattice Parameters Used in the Present Calculations[a]

		Lattice Constants (Å)			Unit-Cell Angles (deg)		
system	crystal symmetry	*a*	*b*	*c*	*α*	*β*	*γ*
TiO_2	anatase	3.785	3.785	9.514	90.0	90.0	90.0
TiO_2	rutile	4.593	4.593	2.959	90.0	90.0	90.0
ZnO	wurtzite	3.249	3.249	5.204	90.0	90.0	120.0
NiO[b]	rock salt	4.173	4.173	4.173	90.0	90.0	90.0
FeO	rock salt	4.332	4.332	4.332	90.0	90.0	90.0
V_2O_5	orthorhombic	11.519	3.564	4.373	90.0	90.0	90.0
WO_3	monoclinic-*γ*	7.297	7.539	7.688	90.0	90.9	90.0
Bi_2O_3	monoclinic-*α*	5.848	8.166	7.509	90.0	113.0	90.0
MoS_2	molybdenite	3.150	3.150	12.300	90.0	90.0	120.0
WS_2	molybdenite	3.180	3.180	12.500	90.0	90.0	120.0
$MoSe_2$	molybdenite	3.287	3.287	12.929	90.0	90.0	120.0
WSe_2[c]	molybdenite	3.280	3.280	12.950	90.0	90.0	120.0
GaN	wurtzite	3.190	3.190	5.189	90.0	90.0	120.0
AlN	wurtzite	3.110	3.110	4.980	90.0	90.0	120.0

[a]Unless specified otherwise, the structures and lattice parameters were taken from ref 40. [b]Data taken from ref 41. [c]Data taken from ref 42.

approximations for the exchange-correlation energy and potential are the local density approximation (LDA) and the generalized gradient approximation (GGA). Despite the great success to predict the structure, stability, and properties of solids and molecules, band-gap energies calculated within LDA or GGA are subject to systematic errors, thus indicating major limitations of DFT for predicting the electronic properties of strongly correlated systems, where the approximate exchange wrongly favors charge delocalization.[20] In the example of the 3D TMOs with rock-salt crystal symmetry, the conventional DFT approximations heavily underestimate the size of the band gap or even incorrectly predict such TMOs to be metals, while they are, in fact, semiconductors or insulators in the experiments.[21−23]

Hybrid DFT methods[24−28] have been widely used to reduce the self-interaction error in the approximate exchange potential. This can be done by mixing the local or semilocal DFT exchange with the exact nonlocal Hartree−Fock (HF) exchange, although the computations become expensive, because of the evaluation of the HF integrals. Alternatively, DFT+*U* theory is a more economical approach, which employs the effective intra-atomic Coulomb parameter (*U*).[29−33] *U* can be obtained fully ab initio from constrained DFT calculations, and it can be tuned to resemble the experimental band-gap energies. For different solid-state materials, however, *U* has different values and must be optimized for each system separately. The most accurate electronic structure calculations available to date are provided by the GW method;[34,35] however, this approach requires very expensive calculations, especially if they are done self-consistently.

The development of XC functionals for electronic structure calculations has been an active field in the past decades. Two examples that have proven to be very successful are the so-called HSE06 XC functional[27,28] (Heyd-Scuseria-Ernzerhof) and the TB-mBJ[36] (Tran-Blaha modified Becke-Johnson) XC potential. HSE06 applies a screened Coulomb potential only to the exchange interaction in order to screen the long-range part of the HF exchange, which results in a reduced computational time, in comparison to the best established hybrid methods, such as B3LYP[37−39] or PBE0.[25] On the other hand, TB-mBJ is

Table 2. Calculated Band Gaps of Selected Systems Using the DFT/PBE Level of Theory and Various Basis Sets

basis set	ZnO	$TiO_{2(A)}$	V_2O_5	Bi_2O_3	MoS_2	WS_2
			Wien2k Software[43]			
(L)APW+lo	0.82	2.16	1.92	2.47	0.87	1.06
			ADF/BAND[a] **Software**[44−46]			
DZ	1.02	1.94	1.64	2.50	0.94	1.04
TZP	0.84	1.97	1.75	2.44	0.90	1.07
TZ2P	0.79	2.06	1.76	2.42	0.88	1.06
			VASP Software[47,48]			
PAW[b]	0.81	1.98 (2.10)	1.76 (1.87)	2.43 (2.44)	0.89	1.06

[a]ADF/BAND results are obtained with *k*-space and integration accuracy set to 4. [b]VASP calculations were carried out using large-core treatment. The numbers shown in parentheses correspond to the VASP calculations with a semi-core scheme.

an orbital-independent XC potential that is dependent solely on semilocal quantities, with accuracy claimed to be comparable to the GW method and computational effort that is as inexpensive as LDA or GGA, bceause of the absence of a nonlocal HF contribution in the XC potential.

In this paper, we present validation calculations on the electronic structure of a large class of en vogue materials—namely, metal and transition-metal oxides (TMOs), transition-metal dichalcogenides (TMDs), and two metal nitrides—in order to determine the best available DFT method that would be easily applicable to screen the electronic structure for a large number of transition-metal-containing materials. The performance of common as well as modern density functionals is discussed, and the results are compared with the available experimental data. We have chosen the TMO and TMD materials due to the fact that they exhibit promising properties for applications in catalytic water splitting and 2D nanoelectronics. We plan to use the presented data as basis for a combinatorial screening of a large number of pure and mixed TMO materials and doped TMD layers, where correct evaluation of the band-edge positions and the band-gap sizes is crucial. We do not discuss the properties of these pure materials in detail here, since they have been studied extensively at various levels of theory (see, e.g., the review paper of Cramer and Truhlar in ref 18 and references therein).

METHODOLOGY

The variety of metal and transition-metal compounds and the crystal symmetries studied in this work are shown in Figure 1. For more-complete validation, we have chosen magnetic and nonmagnetic oxides that are often complex to model. We have studied experimental crystal structures, whose lattice parameters and crystal class symmetries are summarized in Table 1.

First-principles validation calculations were performed on the basis of DFT, as implemented in the following scientific software packages: Wien2k,[43] ADF/BAND,[44−46] VASP,[47,48] and Crystal09.[49] These codes employ rather different numerical approaches for the description of the Bloch functions, including local basis sets and plane waves, as well as for the description of the core electrons, as detailed below.

For the local basis functions, Crystal09 and ADF/BAND use Gaussian- and Slater-type orbitals, respectively. In Crystal09, it is imperative to use Effective Core Potentials (ECP), while ADF/BAND allows the all-electron (AE) methodology, as well as the Frozen Core (FC) treatment with scalar relativistic corrections (ZORA).[50−52] The FC choice in ADF/BAND can be set to small, medium, or large, and the same treatment applies to all elements in the studied system. We have performed calculations using either AE or medium core (see Table S1 in the Supporting Information (SI)).

VASP and Wien2k both approximate the Bloch orbitals by plane-wave expansions, and we have applied PAW (Projector Augmented Waves)[53] and FP-LAPW+lo (Full-Potential Linearized Augmented-Plane Wave with local orbitals)[54−56] methods, respectively. We have set the energy cutoff to 420 eV for the VASP plane-wave calculations. This value has been validated, with respect to the band-gap size and the total energy of the systems. The FP-LAPW+lo method in Wien2k, with its all-electron scheme, is our reference method, while the PAW implementation in VASP, with a large core, was chosen as a computationally low-cost alternative. All Wien2k calculations were carried out fixing the product of $R_{MT} \times K_{max}$ to 7.0, where R_{MT} denotes the smallest muffin tin radius and K_{max} the plane-wave cutoff parameter.

The mesh of *k*-points was obtained according to the scheme proposed by Monkhorst and Pack[57] in VASP and Crystal09, while, for ADF/BAND, the tetrahedra-based mesh of Wiesenekker and Baerends was applied.[58] We have used the improved tetrahedron method for Brillouin-zone integrations in the case of Wien2k.[59] The tetrahedra-based mesh in ADF/BAND is constructed such that, for an even number of *k*-space parameters, the linear tetrahedron method is applied, while for an odd number of parameters, it follows the quadratic tetrahedron method. The Γ-point is used for the *k*-space parameter that has been set to 1. The *k*-point mesh was set to be at least 5 × 5 × 5 for the large-unit-cell materials WO_3 and Bi_2O_3 and 8 × 8 × 8 for all other systems, independent of the choice of the functional.

First, we have studied the influence of the different basis sets, core treatments, and software implementation differences on the band gap (see Table 2) for selected systems. The results show that, for a given XC functional, in this case PBE, all packages perform very similarly with band-gap differences that are much lower than the accuracy one would expect from DFT for these quantities. Concerning the Slater-type bases, the basis set size varies the band gap only slightly and a very good agreement with the plane-wave methods is obtained already for the triple-ζ bases with one polarization function (TZP). Therefore, in the following, we present the ADF/BAND results obtained using TZP basis set, unless specified otherwise. The Gaussian basis functions used for CRYSTAL09 calculations are given in the SI. It is important to note that the differences in the band gaps occurring between both plane-wave methods for $TiO_{2(A)}$ and V_2O_5 originate from the electron treatment of the heavy elements. This is due to the large core used in our PAW calculations. The results are in a better agreement if a more expensive semicore treatment is used.

However, as a computationally low-cost variant, we will keep the large-core PAW method as the default for VASP.

Various XC functionals/potentials are tested as shown in Table 3. The codes offer a rather different choice of XC functionals. While PBE is available to all of them, GGA+U is available in Wien2k, VASP, and ADF/BAND, B3LYP is available only in CRYSTAL, and Wien2k (some calculations also report B3LYP in VASP[60]), PBE0 in VASP and CRYSTAL (now also available in Wien2k[61]), HSE06 only in VASP, and TB-mBJ in ADF/BAND and Wien2k (some calculations also report this functional in VASP[62]). VASP calculations were performed using DFT+U, PBE0, and HSE06 functionals, while PBE, B3LYP, and TB-mBJ were used as implemented in ADF/BAND, Crystal09, and Wien2k (ADF/BAND), respectively.

Table 3. Availability of Selected XC Functionals in Various Computational Codes

software	PBE	GGA+U	PBE0	B3LYP	HSE06	TB-mBJ
Wien2k	×	×	×[a]	×[a]		×
VASP	×	×	×	×[b]	×	×[c]
ADF/BAND	×	×				×
Crystal09	×		×	×		

[a]According to ref 61. [b]As reported in ref 60. [c]As reported in ref 62.

For the DFT+U calculations, we have chosen the simplified scheme suggested by Dudarev et al.[32] with the effective U parameter ($U_{eff} = U - J$, where U is the effective intra-atomic Coulombic energy and J is the exchange energy). The TB-mBJ calculations were performed using the default parameters of the potential, as suggested in the original publication by Tran and Blaha.[36]

The magnetic TMOs (FeO and NiO) were treated using the antiferromagnetic ordering (AF−II), and the resulting magnetic moments for all the density functionals are given Table 4. It is well-known that the standard implementations of DFT, such as PBE, underestimate the magnetic moments of TMOs. For the GGA+U, the magnetic moment increases with increasing U. The estimation of the magnetic moments can also be improved by employing hybrid functionals, as well as with the TB-mBJ potential. The detailed discussion of the magnetic properties is beyond the scope of the present work and, therefore, will not be discussed here.

RESULTS AND DISCUSSION

We have calculated the electronic structures of a wide variety of materials, including metal oxides, chalcogenides, and nitrides, and the resulting band-gap sizes are given in Table 5. As expected, GGA in the standard implementations, as in the widely used PBE functional, generally strongly underestimates the band gaps, ranging from ∼2% error for dichalcogenides up to ∼77% for rock-salt type TMOs. The most striking example is the FeO crystal, which is a well-known Mott insulator, but which is predicted to be metallic by the PBE XC functional due to the wrong treatment of the Fe d-orbitals. This problem is well-known for the (semi)local functionals (see, e.g., ref 63) and it has been recognized already in the 1980s.[64] The situation is slightly improved for the TMOs if the hybrid PBE0 functional is used, although this approach tends to overestimate the band gaps. The errors decrease by up to 50%, compared to pure GGA functionals, and the Mott insulators are correctly converged to an insulating state. However, the estimation of the electronic structure within PBE0 is much worse in the case of TMDs, what we have already reported earlier.[4] In this study, PBE0 has overestimated band-gap energies by up to 80%. For the MoS_2 bulk, Marques et al.[65] have obtained at the same level of theory 2.09 eV band gap, in close agreement to our 2.11 eV. Marques et al. have also studied zinc oxide and nitrides using PBE0. They have obtained band-gap values of 3.26 and 6.25 eV for the ZnO and AlN, respectively. Our results differ only slightly with those of Marques et al., by ∼2.5%. For most of the studied systems, the other hybrid functional, B3LYP, gives band-gap energies similar to those of PBE0, exhibiting the same overestimating behavior. The exception is the AlN, where PBE0 and B3LYP differ by ∼1 eV, most probably due to the choice of basis set of Al.

The DFT+U approach is a convenient tool for tuning the electronic structure in order to obtain band gaps of semiconducting TMOs in very good agreement with experimental data. In principle, one could optimize the U parameter to approach the experimental values of gap energies, as in the example of V_2O_5 (for U = 3 eV, the agreement is almost perfect, with an error of 1.3%). This formalism is not very useful if one would like to apply it for combinatorial screening of a large number of mixed systems, because U differs from system to system. Our results show that, for FeO and NiO, it is much easier to correct the DFT values by optimizing U. In this case, changes from U = 3 eV to U = 4 eV decrease the error by up to 20%. For other materials, e.g., for the ZnO wurtzite structure, this change is very small, and even for large values of U, the experimental band gaps are not approached. This is due to the fact that the d-orbitals of the Zn atoms are fully occupied and, therefore, do not contribute to the frontier states close to the Fermi level. Moreover, there is a hybridization between the d-orbitals of Zn and the p-orbitals of O. The latter will not be strongly affected by the U parameter, leaving the band gap almost unaffected. Also, the U parameter does not really affect the band gaps of TMD materials and changing the value of U by 1 eV results in only ∼2% improvement, yielding band gaps that are still far from the experimental findings. In the case of TMDs, the band gaps are observed between the d-orbitals of the transition-metal atoms. The size of the band gap is dependent strongly on the interlayer distance and is mainly caused by the nonlocal effects (crystal-field splitting), and not

Table 4. Calculated Magnetic Moments (μ_B) of FeO and NiO with Antiferromagnetic Ordering Using Various Density Functionals[a]

		GGA+U						
system	PBE	U = 3	U = 4	U = 5	PBE0	B3LYP	HSE06	TB-mBJ
FeO	3.47	3.61	3.66	3.70	3.62	3.75	3.62	3.63
NiO	1.40	1.56	1.62	1.67	1.66	1.72	1.65	1.75 (1.76)

[a]TB-mBJ results using Wien2k (and ADF/BAND) are given. ADF/BAND calculations were carried out using medium core, k-space, and integration accuracy set to 5. U values are given in eV.

Table 5. Calculated Band-Gap Energies (eV) of Metal Oxides, Chalcogenides, and Nitrides Using Various Density Functionals, in Comparison with Experimental Data and the GW Method[a]

		GGA+U							GW		Experiment	
system	PBE	U = 3	U = 4	U = 5	PBE0	B3LYP	HSE06	TB-mBJ	value	ref	value	ref
$TiO_{2(A)}$[b]	1.94	2.50	2.70	2.92	4.11	4.03	3.38	3.05 (2.74)	3.56	66	3.30	67
$TiO_{2(R)}$[c]	1.64	2.13	2.29	2.48	3.87	3.46	3.12	2.67 (2.32)	3.34	66	3.03	68
ZnO	0.87	1.19	1.31	1.42	3.18	3.30	2.54	2.68 (2.74)	3.20	69	3.30	70
FeO	0.00	1.18	1.57	1.97	3.00	2.97	2.25	1.83 (−)	2.20	71	2.40	72
NiO	0.88	2.20	2.61	3.01	5.19	4.93	4.45	4.14 (4.67)	3.80	73	4.20	74
V_2O_5	1.74	2.28	2.50	2.73	3.98	3.57	3.23	2.87 (2.68)	1.85	75	2.30	76
WO_3	1.79	2.04	2.18	2.31	3.68	2.50	2.94	2.90 (2.76)	2.93	77	2.80	78
Bi_2O_3	2.45	[2.44][d]	[2.44][d]	[2.44][d]	4.11	3.90	3.50	3.36 (3.40)			2.85	79
MoS_2	0.90	0.90	0.91	0.93	2.11	1.93	1.46	1.11 (1.18)	1.23	80	1.23	81
WS_2	1.07	1.07	1.08	1.11	2.25	2.00	1.60	1.31 (1.37)	1.30	80	1.35	81
$MoSe_2$	0.91	0.85	0.85	0.87	2.03		1.36	1.02 (1.05)	1.11	80	1.09	81
WSe_2	0.99	0.96	0.97	0.99	2.06		1.44	1.20 (1.17)	1.19	80	1.20	81
GaN	2.07	[2.14][d]	[2.22][d]	[2.31][d]	3.87	3.79	3.22	3.10 (3.54)	3.35	82	3.50	83
AlN	4.26				6.31	7.33	5.60	5.63 (6.05)	6.14	82	6.20	83
RMS (eV)[e]	1.56	1.05	0.90	0.78	0.90	0.75	0.44	0.38 (0.38)	0.22			
ABE (eV)[f]	3.32	2.11	1.99	1.88	1.68	1.27	0.93	0.62 (0.71)	0.45			

[a]TB-mBJ results using Wien2k (and ADF/BAND) are given. ADF/BAND calculations were carried out using medium core, k-space, and integration accuracy set to 5. U values are given in eV. [b]Anatase phase. [c]Rutile phase. [d]For Bi and Ga, only s- and p-orbitals are available in the valence shell. Therefore, GGA+U calculations can only be performed using the semicore scheme, thus involving explicit treatment of the d-orbitals (and, for Bi, also f-orbitals). [e]Root-mean-square deviation. [f]Absolute error.

by the strong on-site Coulomb interactions. Therefore, GGA +U will not improve the band gap of TMDs, because this method is only a local correction that can affect localized electrons.

We have tested two modern XC approaches that have been designed to improve DFT band gaps, namely, the screened hybrid HSE06 functional and semilocal TB-mBJ potential. Our results show agreement with the experimental data within ~25% maximum error (and typically <10%). Comparing our results with those reported by Marques et al.[65] for MoS_2, ZnO, and AlN, we have found a very good agreement at the HSE06 level. We have calculated the band gaps for these materials as 1.46, 2.54, and 5.60 eV, respectively, in perfect agreement with Marques et al., who obtained values of 1.42, 2.57, and 5.53 eV. The comparison of various XC functionals with experimental data for selected materials is also shown in Figure 2.

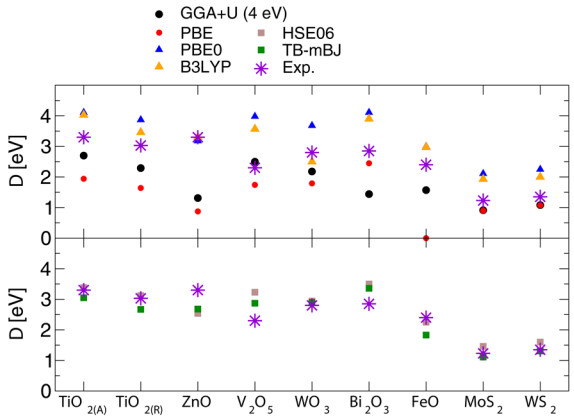

Figure 2. Calculated band gaps of metal oxides and chalcogenides using various density functionals, in comparison with the experimental values. See text and Table 5 for more details.

For the calculations of band gaps using the TB-mBJ potential, we have observed rather strong differences, reaching up to 0.7 eV between FP-LAPW+lo and the local basis set methods. Closer examination of the results indicates dependency on the Slater-type basis sets and the frozen-core approximation (see Table S1 in the SI). For example, the medium frozen-core treatment in ADF/BAND is not sufficient for metal oxides such as TiO_2, NiO, or V_2O_5, and it is necessary to include more electrons that are treated explicitly.[84] The size of the basis set typically has an influence of up to 200 meV; however, for special cases, such as NiO, the convergence is not reached, even with the QZ4P (quadrupole-ζ bases with four polarization functions). In general, however, error bars of the TZP basis with respect to the experiment do not differ significantly from those of the FP-LAPW+lo reference method.

The electronic band structures and the corresponding projected densities of states (PDOS) of all of the studied materials are shown in Figures 3 and 4, respectively. They have been carried out using the TB-mBJ functional as implemented in Wien2k (reference calculations). All studied materials can be divided into two groups according to the band gaps: (1) direct band gap at Γ is found for ZnO, $TiO_{2(R)}$, AlN, and GaN, while (2) indirect band gap is obtained for all the other crystal structures. TMD materials have a valence band maximum (VBM) occurring at the Γ point with a transition to the conduction band minimum (CBM) observed halfway between Γ and K. This is in a close agreement with our previous results obtained using the PBE functional.[4]

The band structures of TMO materials are much more complicated, and there is no clear trend about the occurrence of VBM and CBM. For example, anatase ($TiO_{2(A)}$) and rutile ($TiO_{2(R)}$) differ significantly in their electronic structure: while the band-gap difference is only ~0.3 eV, the dispersion of the bands is much stronger in the case of rutile. In agreement with the experimental findings and results from other theoretical works, we have obtained the direct band gap at the Γ point for

dx.doi.org/10.1021/ct400235w | J. Chem. Theory Comput. 2013, 9, 2950−2958

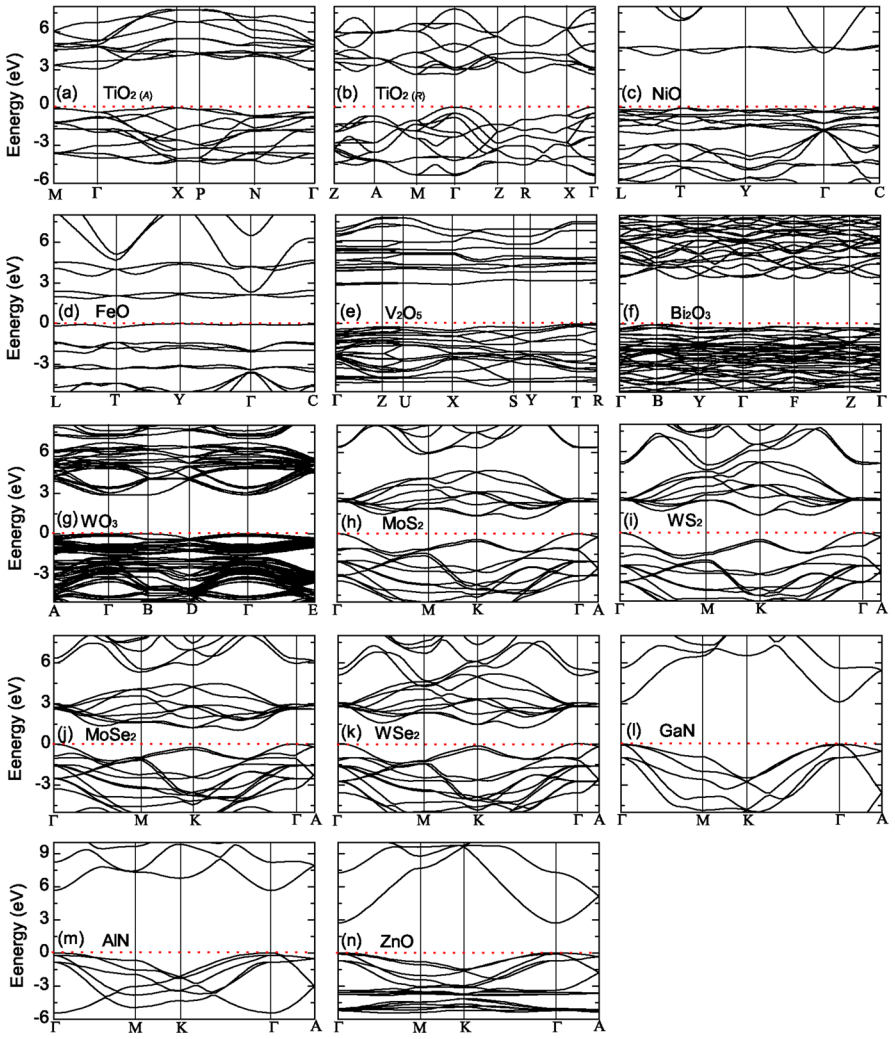

Figure 3. Electronic band structures calculated using the TB-mBJ XC functional and plane-wave basis sets as implemented in Wien2k. The dashed horizontal lines denote the Fermi level that was shifted to the top of the valence band.

rutile, while anatase is an indirect band gap semiconductor, where the transition occurs between the X and Γ points along the Δ-direction.[85−87]

In the example of the rock-salt mono-oxides, such as FeO and NiO, the band structure close to the Fermi level is dominated by dispersion-less d-bands. Here, the VBM and CBM are found at different *k*-points: for FeO, the VBM is found at the Y high-symmetry point, while the CBM is located between Y and Γ.[88,89] In the case of NiO, the VBM is located at T, while the CBM is exactly between points L and T.[89,90]

The PDOS is much more informative, compared to the band structure when discussing the band-gap origins. For many systems studied in the present work, the VB close to the Fermi level is dominated by O 2p states (TiO_2, V_2O_5, WO_3, AlN, and GaN), while the CB is composed either of the transition-metal d-orbitals (TiO_2, V_2O_5) or the mixture of these states with the O/N 2p states.

Our PDOS calculations describe NiO and FeO as Mott−Hubbard insulators, because of the band gaps that occur between the transition-metal 3d-orbitals. The VBM of Ni and Fe atoms show a pronounced 3d density with minor contributions from O 2p states. The CBM is also composed of Fe/Ni 3d with even less density of the O 2p orbitals. This is in very good agreement with the work of Koller et al.[90] for NiO at the same level of theory and with the work of Anisimov et al. for FeO.[89] Moreover, for these two oxides, there is a very small contribution to the VBM and CBM originating from the transition-metal 4s-orbitals, which, depending on the XC functional used in the calculation, might be important. We have also calculated the PDOS of FeO, TiO_2, Bi_2O_3, and WO_3, using the HSE06 functional. The band structures of these materials are given in Figure S1 in the SI. While the PDOS plots of TiO_2, Bi_2O_3, and WO_3 give the same results with both XC functionals, we find changes in the electronic structure of FeO, which result in the well-known conclusion that this mono-oxide is, in fact, not a Mott−Hubbard insulator but rather a charge-transfer insulator. The CBM is composed of Fe and O s-states (with a ratio of ∼55% to 45%), and the dispersionless 3d states are found only above them. This is in a very good agreement with the recent work of Rödl et al.,[71] who have studied FeO using the HSE03+GW method. Historically, the rock-salt mono-oxides in the paramagnetic phase were assumed to be examples of prototypical Mott−Hubbard insulators.[91] However, experimental methods, such as X-ray photoemission spectroscopy (XPS) or Bremsstrahlung isochromat spectroscopy (BIS), are not conclusive either.[92,93]

ZnO is yet another mono-oxide with a wurtzite crystal symmetry. It is a direct band gap semiconductor at the Γ point

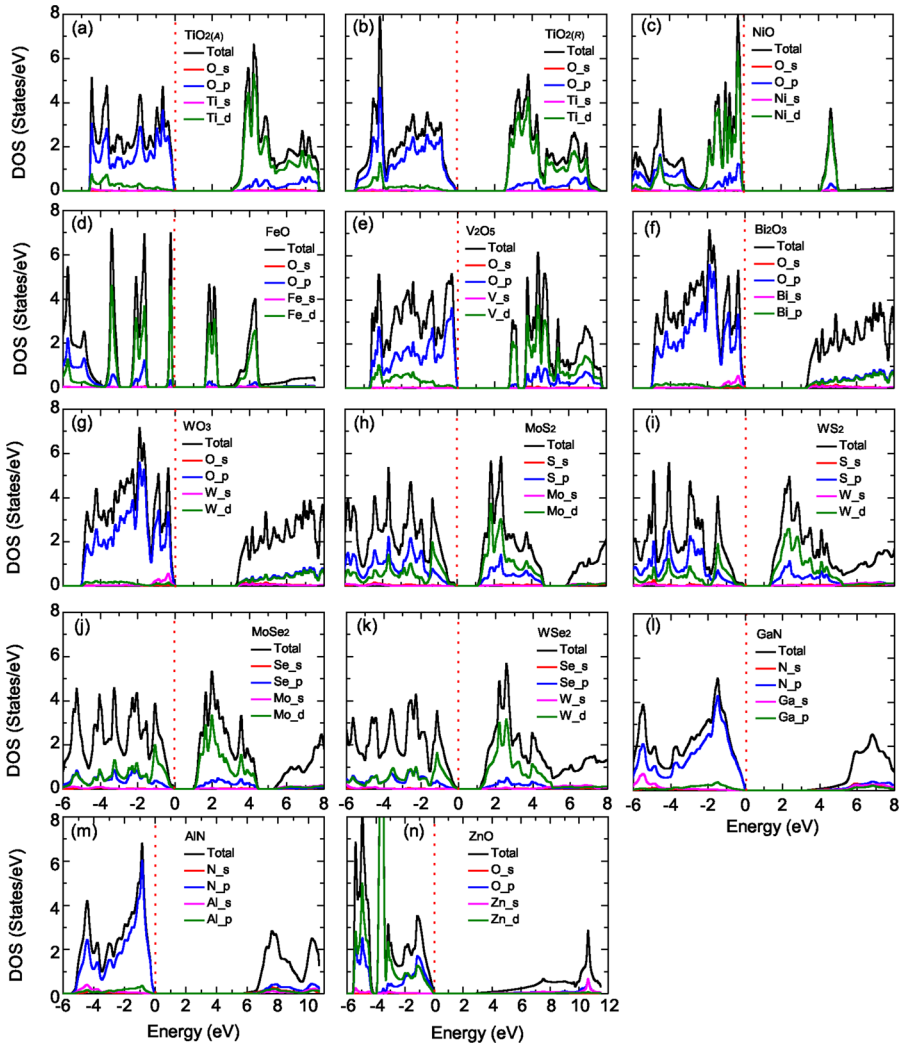

Figure 4. Orbital-projected densities of states calculated using the TB-mBJ XC functional and plane-wave basis sets as implemented in Wien2k. The dashed vertical lines denote the Fermi level that was shifted to the top of the valence band. Note the differences in the scaling of the energy axis.

and the band edges are dominated by O 2p and Zn 3d states for VBM and CBM, respectively. Moreover, the VBM has a significant contribution from the Zn 3d states, resulting in a strong hybridization with the oxygen states. Our results agree perfectly with the work of Singh et al.[94] at the same level of theory.

Finally, we have compared the band structure and PDOS calculated for TiO_2, MoS_2, and ZnO using the PBE, GGA+U (U = 4 eV), HSE06 functionals, and the TB-mBJ potential. As expected from the band gaps, there are noticeable changes in the electronic structure, particularly in the conduction band. The results are given in Figures S2 and S3 in the SI.

CONCLUSIONS

We have studied the performance of various exchange correlation functionals and periodic implementations of density functional theory (DFT) in order to compute the band gaps and electronic structure of a series of transition-metal oxide, nitride, and chalcogenide compounds (i.e., systems that have been known to be problematic for band-gap estimations using DFT). Our principal result is that, although the performance of DFT within GGA and hybrid functionals is well-known to be insufficient to solve this problem, one can obtain band gaps with semilocal functionals with an appreciable accuracy of ~25% using modern exchange-correlation functionals/potentials that have been optimized for predicting electronic structures (namely, HSE06 and TB-mBJ). These results are not globally competitive, with regard to accuracy, with the GW method and they certainly are not good enough to match experimental results closely; however, they are indeed sufficient to provide a combinatorial screening of a large range of composite materials at low computational cost. The band structures and PDOS are in rather close agreement with available reference data from the literature.

We have also found a dependency of the band-gap values on the Slater-type basis sets and the frozen-core approximation for the TB-mBJ potential, for oxides such as NiO, in contrast to the GGA, and these results should be further explored. If the semicore approach is taken into account, we have observed a better agreement between the results from the local basis and the plane waves.

Our results show that both local-basis functions and plane-wave methods are equally suitable for these types of calculations. It should be noted that (i) unfortunately, not all functionals are available in the most widespread solid-state software packages, and (ii) there is still room for improvement of the density functionals, in terms of band-gap sizes.

■ ASSOCIATED CONTENT

Supporting Information

Validation calculations using TB-mBJ potential in ADF/BAND, partial densities of states of FeO, TiO_2, Bi_2O_3 and WO_3 calculated at the DFT/HSE06 level, and comparison of electronic band structure and PDOS calculated at selected DFT levels for MoS_2, rutile ($TiO_{2(R)}$), and ZnO are provided. This material is available free of charge via the Internet at http://pubs.acs.org.

■ AUTHOR INFORMATION

Corresponding Author

*E-mail: a.kuc@jacobs-university.de.

Notes

The authors declare no competing financial interest.

■ ACKNOWLEDGMENTS

Financial support by the Marie-Curie Actions FP7-PEOPLE-2009-IAPP (QUASINANO) and FP7-PEOPLE-2012-ITN (PROPAGATE), and the German Research Council (Deutsche Forschungsgemeinschaft) in Priority Program SPP 1613 is gratefully acknowledged. The authors thank Dr. P. Philipsen and Dr. F. Tran for their technical support and helpful discussions.

■ REFERENCES

(1) Parr, R. G.; Yang, W. *Density-Functional Theory of Atoms and Molecules*; Oxford University Press: Cambridge, U.K., 1989; Vol. *16*.
(2) Kohn, W. *Rev. Mod. Phys.* **1999**, *71*, 1253−1266.
(3) Coleman, J. N.; et al. *Science* **2011**, *331*, 568−571.
(4) Kuc, A.; Zibouche, N.; Heine, T. *Phys. Rev. B* **2011**, 245213-1−245213-4.
(5) Radisavljevic, B.; Radenovic, A.; Brivio, J.; Giacometti, V.; Kis, A. *Nat. Nanotechnol.* **2011**, *6*, 147−150.
(6) Radisavljevic, B.; Whitwick, M. B.; Kis, A. *ACS Nano* **2011**, *5*, 9934−9938.
(7) Radisavljevic, B.; Whitwick, M. B.; Kis, A. *Appl. Phys. Lett.* **2012**, *101*, 043103-1−043103-4.
(8) Fujishima, A.; Honda, K. *Nature* **1972**, *238*, 37−38.
(9) Kudo, A.; Miseki, Y. *Chem. Soc. Rev.* **2009**, *38*, 253−278.
(10) Coelho, B.; Oliveira, A. C.; Mendes, A. *Energy Environ. Sci.* **2010**, *3*, 1398−1405.
(11) Shen, S.; Shi, J.; Guo, P.; Guo, L. *Int. J. Nanotechnol.* **2011**, *8*, 523−591.
(12) Siegbahn, P. E. M. *Chem. Phys. Lett.* **1993**, *201*, 15−23.
(13) Siegbahn, P. E. M.; Svensson, M. *Chem. Phys. Lett.* **1993**, *216*, 147−154.
(14) Gutsev, G. L.; Andrews, L.; Bauschlicher, C. W. *Theor. Chem. Acc.* **2003**, *109*, 298−308.
(15) Wang, X.; Zhang, F. X.; Loa, I.; Syassen, K.; Hanfland, M.; Mathis, Y. L. *Phys. Status Solidi B* **2004**, *241*, 3168−3178.
(16) Errico, L. A.; Renteria, M.; Weissmann, M. *Phys. Rev. B* **2005**, *72*, 184425-1−184425-8.
(17) Kane, M. H.; Fenwick, W. E.; Strassburg, M.; Nemeth, B.; Varatharajan, R.; Song, Q.; Keeble, D. J.; El-Mkami, H.; Smith, G. M.; Zhang, Z. J.; Nause, J.; Summers, C. J.; Ferguson, I. T. *Phys. Status Solidi B* **2007**, *244*, 1462−1467.
(18) Cramer, C. J.; Truhlar, D. G. *Phys. Chem. Chem. Phys.* **2009**, *11*, 10757−10816.
(19) Mehtougui, N.; Rached, D.; Khenata, R.; Rached, H.; Rabah, M.; Bin-Omran, S. *Mater. Sci. Semicond. Process.* **2012**, *15*, 331−339.
(20) Cohen, A. J.; Mori-Sanchez, P.; Yang, W. *Science* **2008**, *321*, 792−794.
(21) Zaanen, J.; Sawatzky, G. A.; Allen, J. W. *Phys. Rev. Lett.* **1985**, *55*, 418−421.
(22) Hufner, S. *Adv. Phys.* **1994**, *43*, 183−356.
(23) Anisimov, V. I.; Aryasetiawan, F.; Lichtenstein, A. I. *J. Phys.: Condens. Matter* **1997**, *9*, 767−808.
(24) Becke, A. D. *J. Chem. Phys.* **1993**, *98*, 1372−1377.
(25) Perdew, J. P.; Emzerhof, M.; Burke, K. *J. Chem. Phys.* **1996**, *105*, 9982−9985.
(26) Adamo, C.; Barone, V. *Chem. Phys. Lett.* **1997**, *274*, 242−250.
(27) Heyd, J.; Scuseria, G. E.; Ernzerhof, M. *J. Chem. Phys.* **2003**, *118*, 8207−8215.
(28) Heyd, J.; Scuseria, G.; Ernzerhof, M. *J. Chem. Phys.* **2006**, *124*, 219906-1−.
(29) Anisimov, V. I.; Zaanen, J.; Andersen, O. K. *Phys. Rev. B* **1991**, *44*, 943−954.
(30) Czyzyk, M. T.; Sawatzky, G. A. *Phys. Rev. B* **1994**, *49*, 14211−14228.
(31) Liechtenstein, A. I.; Anisimov, V. I.; Zaanen, J. *Phys. Rev. B* **1995**, *52*, R5467−R5470.
(32) Dudarev, S. L.; Botton, G. A.; Savrasov, S. Y.; Humphreys, C. J.; Sutton, A. P. *Phys. Rev. B* **1998**, *57*, 1505−1509.
(33) Cococcioni, M.; de Gironcoli, S. *Phys. Rev. B* **2005**, *71*, 035105-1−035105-16.
(34) Hedin, L. *Phys. Rev.* **1965**, *139*, A796−A823.
(35) Aulbur, W. G.; Stadele, M.; Gorling, A. *Phys. Rev. B* **2000**, *62*, 7121−7132.
(36) Tran, F.; Blaha, P. *Phys. Rev. Lett.* **2009**, *102*, 226401-1−226401-4.
(37) Becke, A. D. *J. Chem. Phys.* **1993**, *98*, 5648−5652.
(38) Lee, C. T.; Yang, W. T.; Parr, R. G. *Phys. Rev. B* **1988**, *37*, 785−789.
(39) Vosko, S. H.; Wilk, L.; Nusair, M. *Can. J. Phys.* **1980**, *58*, 1200−1211.
(40) Crystallographic and Crystallochemical Database for Minerals and Their Structural Analogues, http://database.iem.ac.ru/mincryst/, accessed 2013.
(41) Brownlee, L. D.; Mitchell, E. W. J. *Proc. Phys. Soc., London, Sect. B* **1952**, *65*, 710−716.
(42) Coehoorn, R.; Haas, C.; Dijkstra, J.; Flipse, C. J. F.; Degroot, R. A.; Wold, A. *Phys. Rev. B* **1987**, *35*, 6195−6202.
(43) Blaha, P.; Schwarz, K.; Madsen, G. K. H.; Kvasnicka, D.; Luitz, J. *Wien2k, An Augmented Plane Wave Plus Local Orbitals Program for Calculating Crystal Properties*; Vienna University of Technology, Austria, 2001.
(44) Philipsen, P. H. T.; te Velde, G.; Baerends, E. J.; Berger, J. A.; de Boeij, P. L.; Groeneveld, J. A.; Kadantsev, E. S.; Klooster, R.; Kootstra, F.; Romaniello, P.; Skachkov, D. G.; Snijders, J. G.; Wiesenekker, G.; Ziegler, T. *BAND2012*. SCM, Theoretical Chemistry, Vrije Universiteit, Amsterdam, The Netherlands, http://www.scm.com, accessed 2012.
(45) Wiesenekker, G.; Baerends, E. J. *J. Phys.: Condens. Matter* **1991**, *3*, 6721−6742.
(46) Velde, G. T.; Baerends, E. J. *Phys. Rev. B* **1991**, *44*, 7888−7903.
(47) Kresse, G.; Hafner, J. *Phys. Rev. B* **1993**, *47*, 558−561.
(48) Kresse, G.; Hafner, J. *Phys. Rev. B* **1994**, *49*, 14251−14269.
(49) Dovesi, R.; Saunders, V. R.; Roetti, R.; Orlando, R.; Zicovich-Wilson, C. M.; Pascale, F.; Civalleri, B.; Doll, K.; Harrison, N. M.; Bush, I. J.; D'Arco, P.; Llunell, M. CRYSTAL09 User's Manual; University of Torino: Torino, Italy, 2009.
(50) van Lenthe, E.; Baerends, E. J.; Snijders, J. G. *J. Chem. Phys.* **1994**, *101*, 9783−9792.
(51) van Lenthe, E.; van Leeuwen, R.; Baerends, E. J.; Snijders, J. G. *Int. J. Quantum Chem.* **1996**, *57*, 281−293.
(52) van Lenthe, E.; Ehlers, A.; Baerends, E. J. *J. Chem. Phys.* **1999**, *110*, 8943−8953.
(53) Blöchl, P. E. *Phys. Rev. B* **1994**, *50*, 17953−17979.
(54) Andersen, O. K. *Phys. Rev. B* **1975**, *12*, 3060−3083.
(55) Sjöstedt, E.; Nordström, L.; Singh, D. *Solid State Commun.* **2000**, *114*, 15−20.
(56) Madsen, G. K. H.; Blaha, P.; Schwarz, K.; Sjöstedt, E.; Nordström, L. *Phys. Rev. B* **2001**, *64*, 195134-1−195134-9.
(57) Monkhorst, H. J.; Pack, J. D. *Phys. Rev. B* **1976**, *13*, 5188−5192.

(58) Wiesenekker, G.; Baerends, E. J. *J. Phys.: Condens. Matter* **1991**, *3*, 6721−6742.
(59) Blochl, P. E.; Jepsen, O.; Andersen, O. K. *Phys. Rev. B* **1994**, *49*, 16223−16233.
(60) Paier, J.; Marsman, M.; Kresse, G. *J. Chem. Phys.* **2007**, *127*, 024103−1−10.
(61) Tran, F.; Blaha, P. *Phys. Rev. B* **2011**, *83*, 235118−1−13.
(62) Kim, Y.-S.; Marsman, M.; Kresse, G.; Tran, F.; Blaha, P. *Phys. Rev. B* **2010**, *82*, 205212-1−205212-11.
(63) El-Mellouhi, F.; Brothers, E. N.; Lucero, M. J.; Bulik, I. W.; Scuseria, G. E. *Phys. Rev. B* **2013**, *87*, 035107-1−035107-11.
(64) Terakura, K.; Oguchi, T.; Williams, A. R.; Kubler, J. *Phys. Rev. B* **1984**, *30*, 4734−4747.
(65) Marques, M. A. L.; Vidal, J.; Oliveira, M. J. T.; Reining, L.; Botti, S. *Phys. Rev. B* **2011**, *83*, 035119-1−035119-5.
(66) Kang, W.; Hybertsen, M. S. *Phys. Rev. B* **2010**, *82*, 085203-1−085203-11.
(67) Tang, H.; Berger, H.; Schmid, P. E.; Levy, F.; Burri, G. *Solid State Commun.* **1993**, *87*, 847−850.
(68) Pascual, J.; Camassel, J.; Mathieu, H. *Phys. Rev. Lett.* **1977**, *39*, 1490−1493.
(69) Shishkin, M.; Marsman, M.; Kresse, G. *Phys. Rev. Lett.* **2007**, *99*, 246403-1−246403-4.
(70) Srikant, V.; Clarke, D. R. *J. Appl. Phys.* **1998**, *83*, 5447−5451.
(71) Rödl, C.; Fuchs, F.; Furthmüller, J.; Bechstedt, F. *Phys. Rev. B* **2009**, *79*, 235114−1−8.
(72) Bowen, H. K.; Adler, D.; Auker, B. H. *J. Solid State Chem.* **1975**, *12*, 355−359.
(73) Faleev, S. V.; van Schilfgaarde, M.; Kotani, T. *Phys. Rev. Lett.* **2004**, *93*, 126406−1−4.
(74) Zimmermann, R.; Steiner, P.; Claessen, R.; Reinert, F.; Hufner, S.; Blaha, P.; Dufek, P. *J. Phys.: Condens. Matter* **1999**, *11*, 1657−1682.
(75) Lany, S. *Phys. Rev. B* **2013**, *87*, 085112-1−085112-9.
(76) Cogan, S. F.; Nguyen, N. M.; Perrotti, S. J.; Rauh, R. D. *J. Appl. Phys.* **1989**, *66*, 1333−1337.
(77) Johansson, M. B.; Baldissera, G.; Valyukh, I.; Persson, C.; Arwin, H.; Niklasson, G. A.; Österlund, L. *J. Phys.: Condens. Matter* **2013**, *25*, 205502-1−205502-11.
(78) Enesca, A.; Andronic, L.; Duta, A.; Manolache, S. *Rom. J. Inf. Sci. Technol.* **2007**, *10*, 269−277.
(79) Qiu, Y.; Yang, M.; Fan, H.; Zuo, Y.; Shao, Y.; Xu, Y.; Yang, X.; Yang, S. *Crystengcomm* **2011**, *13*, 1843−1850.
(80) Jiang, H. *J. Phys. Chem. C* **2012**, *116*, 7664−7671.
(81) Kam, K. K.; Parkinson, B. A. *J. Phys. Chem.* **1982**, *86*, 463−467.
(82) Schleife, A.; Fuchs, F.; Roedl, C.; Furthmueller, J.; Bechstedt, F. *Appl. Phys. Lett.* **2009**, *94*, 012104-1−012104-3.
(83) Vurgaftman, I.; Meyer, J. R. *J. Appl. Phys.* **2003**, *94*, 3675−3696.
(84) El-Mellouhi, F.; Brothers, E. N.; Lucero, M. J.; Scuseria, G. E. *Phys. Rev. B* **2011**, *84*, 115122-1−115122-12.
(85) Serpone, N.; ZLawless, D.; Khairutdinov, R. *J. Phys. Chem.* **1995**, *99*, 16646−16654.
(86) Kavan, L.; Grätzel, M.; Gilbert, S. E.; Klemenz, C.; Scheel, H. J. *J. Am. Chem. Soc.* **1996**, *118*, 6716−6723.
(87) Sai, G.; Bang-Gui, L. *Chin. Phys. B* **2012**, *21*, 057104-1−057104-7.
(88) Tran, F.; Blaha, P.; Schwarz, K.; Novak, P. *Phys. Rev. B* **2006**, *74*, 155108-1−155108-10.
(89) Anisimov, V. I.; Korotin, M. A.; Kurmaev, E. Z. *J. Phys.: Condens. Matter* **1990**, *2*, 3973−3987.
(90) Koller, D.; Tran, F.; Blaha, P. *Phys. Rev. B* **2011**, *83*, 195134-1−195134-10.
(91) Brandow, B. H. *Adv. Phys.* **1977**, *26*, 651−808.
(92) Vanelp, J.; Potze, R. H.; Eskes, H.; Berger, R.; Sawatzky, G. A. *Phys. Rev. B* **1991**, *44*, 1530−1537.
(93) Hufner, S.; Steiner, P.; Sander, I.; Reinert, F.; Schmitt, H. *Z. Phys. B—Condens. Matter* **1992**, *86*, 207−215.
(94) Singh, D. J. *Phys. Rev. B* **2010**, *82*, 205102-1−205102-10.